The 3D Electrical Structure of the Australian Lithosphere

Thesis submitted in accordance with the requirements of the University of Adelaide for an Honours Degree in Geophysics

Andrew Jon May

November 2013

THE UNIVERSITY of ADELAIDE

THE 3D ELECTRICAL STRUCTURE OF THE AUSTRALIAN LITHOSPHERE

ABSTRACT

The broad-scale electrical resistivity structure of the Australian continent is poorly known due to the lack of continent-wide observations. These observations are used to constrain lithospheric conduction and petrophysical conditions. In this study, models of electrical resistivity are developed using various constraints, and these are tested against known observations. Three approaches have been employed. Firstly, using the AWAGS array of 58 magnetotelluric sites across Australia spaced approximately 500 km apart, I analyse geomagnetic depth sounding induction vector data, which are then compared with the broad-scale tectonic components of Australia. Secondly, I have developed an upper crustal and surrounding ocean model of electrical conductance using ocean depth information (ETOPO1) and depth to Proterozoic basement (SEEBASE) with a spatial resolution of approximately 17 km. Thirdly, estimates of seismic shear wave velocity of the lithosphere from 50 to 200 km depth from the AuSREM data, at a spatial resolution of approximately 50 km, were converted to electrical resistivity using an empirical relationship. The induction vectors were then compared with three dimensional modelling developed through two approaches. To good approximation I have been able to demonstrate, that the observed AWAGS induction vector data are explained to first order by the conduction of the oceans and sedimentary basins. Second-order effects of resistivity variations in the deeper lithosphere are significant, but induction vectors are less sensitive to these. Finally, I demonstrate from a 3D inversion of the observed AWAGS data that there are additional crustal conductors that cannot be explained from sediment thickness alone, but require additional conduction mechanisms in the crust over significant depths.

KEYWORDS

Electrical resistivity, conductance, lithosphere, Australia

Table of Contents

LIST OF FIGURES AND TABLES

INTRODUCTION

The Australian continent has experienced a long and complex tectonic history (Betts et al. 2002). Imaging the internal structure and mapping of the lithosphere allows us to better understand existing uncertainties such as the physical state of the crust and upper mantle, the hydration state, lithospheric formation and deformation history (Jones 1999, Jones et al. 2012, Selway 2013). The use of magnetotellurics (MT) and geomagnetic depth sounding (GDS) allows us to image the electrical conductivity on a continental scale (e.g. Evans et al. 2011, Jones et al. 2005, Bedrosian and Feucht 2013) providing important constraints on the physical, chemical and thermal structure of the Australian lithosphere.

Lithospheric properties are observed through various laboratory studies (Wang et al. 2006, Yoshino et al. 2006, Yoshino et al. 2009, e.g. Jones et al. 2012), as well as petrological analysis of mantle xenoliths and seismic data (Jones et al. 2009). Other deep geophysical studies include Kennett et al. (2011)the study of the Australian lithosphere using seismic data sets to map the depth of the Australian Moho by Kennett et al. (2011) and a study of the Australian mantle conducted by Fishwick and Rawlinson (2012).

Recent regional scale MT work conducted in Australia includes studies conducted beneath the Olympic Dam iron oxide copper-gold deposit by Heinson et al. (2006), and a study conducted by Thiel and Heinson (2013) across the Gawler Craton in order to provide constraints on tectonothermal events dating from the Proterozoic.

At the continental scale, major MT studies include the South African Magnetotelluric Experiment (SAMTEX) (e.g. Evans et al. 2011), a study which involved over 700 stations in the Kaapvaal craton, a region in Southern Africa. Through the SAMTEX experiment the authors have shown that the lithospheric mantle contains complex structures with large variations in maximum resistivity at depths of 200-250 km. The study was able to determine that beneath the Bushveld complex, the mantle is highly conductive. Potential causes of this highly conductive region include graphite, sulphide and/or iron metals which were associated with the Bushveld magmatic event (Evans et al. 2011).

Continental scale studies have been conducted in Northern America using data from the USArray project, a component of the EarthScope program in which a series of both permanent and portable MT stations have been placed throughout the United States, covering over 35 % of the continent (Bedrosian and Feucht 2013). Through this project, numerous studies have been conducted (e.g. Evans et al. 2011, Zhdanov et al. 2011, Kelbert et al. 2012, Shen et al. 2013). Most recently, the work of Bedrosian and Feucht (2013), has provided a comprehensive overview of the structure and tectonics of the north-western United States. Modelling by Bedrosian and Feucht (2013) was able to provide constraints on the distribution of fluids and melt within the lithosphere, and it produced a three-dimensional resistivity model that provides insights into the tectonic assembly of Western North America from the Archean to the present.

.

In this study, I aim to use GDS induction data (e.g. Chamalaun and Barton 1990, Chamalaun and Barton 1993, Milligan et al. 1993, Welsh et al. 1996), as well as lithospheric-scale shear wave velocity, depth to crystalline basement, and water depth databases to assess what can be learnt about the physical, chemical and thermal structure of the Australian lithosphere.

BACKGROUND

The Australian continent itself can be broadly split into three zones, the Archean Shield in the west, Proterozoic cratons in central Australia and the Phanerozoic fold belts in the East. Lithospheric growth occurred via vertical and horizontal accretion (Betts et al. 2002), in three major episodes, each comprising approximately one third of the continental area (Kennett et al. 2011). The Proterozoic was a major period of crustal growth in which components of the North Australia, West Australian and South Australian cratons were formed and amalgamated (Betts et al. 2002). The internal structure of the continental lithosphere provides vital insights into its creation and development (Jones 1999). Imaging of the internal structure is analysed through the use of seismic and electromagnetic methods. Knowledge of the internal structure as well as the geometry of the lithosphere-asthenosphere boundary is critically important for developing our understanding of the dynamics of the Earth (Jones 1999, Selway 2013).

The lithosphere is defined as a strong layer at the surface and includes both the crust and shallow upper mantle (Karato 2010). It forms a rigid mechanical boundary and is underlain by a weak layer, the asthenosphere, which is characterised by plastic deformation over large time periods (Eaton et al. 2009). The chemistry of the mantle is dominated by olivine (Pommier 2013). Other major phases found in the lithosphere

include pyroxene and garnet, average trends of mantle composition suggest that the mantle becomes increasingly depleted in incompatible elements (such as Fe, Al , Ca, and radioactive elements) with increasing age (Poudjom Djomani et al. 2001).
The crust forms an integral piece of the lithosphere, and its thickness also plays a major role in controlling the overall behaviour of the lithospheric formation to deformation (Kennett and Salmon 2012).Thin and thick crust provide major contrasting differences in that thin crust allows deformation to be localised in the mantle, whereas thick crust allows stress accumulation within the crust (Kennett and Salmon 2012).

The lithosphere is non-convecting and as such is characterised by conductive geotherms, although in some cases local magmatic activity has the potential to produce a temporary advective geotherm (Y. O'Relly and Griffin 1985). The lithosphere-asthenosphere boundary (LAB) represents the base of the Earth's lithosphere and is governed by a conductive thermal regime, which is isolated from the convecting asthenosphere (O'Reilly and Griffin 2010). The LAB is a moveable boundary, becoming shallower due to thermal and chemical erosion of the lithosphere and deeper through processes such as subcretion of upwelling hot mantle plumes (O'Reilly and Griffin 2010).

Constraining the hydration state of the upper mantle is critical for understanding the dynamics and geochemical evolution of the Australian continent (Yoshino et al. 2009). The presence of water in nominally anhydrous minerals (NAM) has an effect on a number of physical and chemical properties of mantle minerals, in particularly enhancing electrical conductivity (Peslier et al. 2010). Hydrogen can be incorporated

into olivine, a major mineral phase in the mantle, and as such creates a hydrous olivine which has a much higher conductivity when compared with anhydrous olivine (Yoshino et al. 2006).

The rheological properties of Earth's mantle control a number of important geological processes within the upper mantle such as the style of mantle convection and the nature of thermal evolution (Karato 2010). Direct estimations of rheological properties are sourced from deformation experiments on rocks conducted in laboratories under realistic/in-Earth pressure and temperatures (Karato and Wu 1993, Karato 2010). Lithospheric properties are determined through various laboratory studies (e.g. Yoshino et al. 2006, Yoshino et al. 2009, Jones et al. 2012), as well as petrological analysis of mantle xenoliths and seismic data (Jones et al. 2009). The use of deep geophysical studies provides another insight into the complex nature of the lithosphere which laboratory studies cannot necessarily provide.

Many of the above mentioned lithospheric properties have an effect on the electromagnetic responses recorded with MT. There are a number of critical factors which affect electrical resistivity of the lithospheric mantle. Of these factors, resistivity is governed, to the first order, by temperature variation, with a number of other variables including chemistry, rheology and the hydration state (Fullea et al. 2011).

THEORY

The MT method is a passive geophysical technique, which is used to image the electrical resistivity structure of the Earth's crust and its upper mantle through the measurement of time varying natural magnetic fields and the induced electric fields (Simpson and Bahr 2005, Chave and Jones 2012). The MT theory is well established and has been in routine use since 1969 (Chave and Jones 2012). Detailed MT theory, discussions and fundamental equations can be found in reviews and text books, for example Vozoff (1990), Simpson and Bahr (2005) and Chave and Jones (2012).

MT is a natural source electromagnetic (EM) method within the bandwidth of 0.001 s to 10,000 s. Through the penetration of EM waves into the Earth's crust, currents are induced in electrically conductive bodies. These currents then produce secondary magnetic fields and through isolating these, the resistivity distribution associated with the bodies of current can be mapped. The penetration depth is controlled by the skin-depth (Simpson and Bahr 2005), δ (metres), of the sounding, according to the equation

$$\delta = \sqrt{2/\mu_0 \omega \sigma} \tag{1}$$

where ω is the angular frequency in radians of the external field, μ_0 is the free air permeability ($4\pi \,.\, 10^{-7}\, Hm^{-1}$), and σ is the conductivity of the medium in Siemens per metre. This equation can then be simplified to

$$\delta \approx 500\sqrt{\rho T} \tag{2}$$

where ρ is the resistivity in Ohm metres (Ω.m) and T is the period (Arora et al. 1999).

Induction vectors are derived from transfer functions that relate the vertical magnetic field to the horizontal magnetic field, represented by the following equation:

$$B_z = T_{zx} B_x + T_{zy} B_y \tag{3}$$

where T_{zx} and T_{zy} are the complex valued transfer functions and B_x, B_y and B_z form the three components of the geomagnetic field.

Lateral resistivity changes can be shown by the use of the GDS induction vectors, sometimes known as Parkinson induction arrows (Simpson and Bahr 2005). When considering laterally uniform resistivity, there is no anomalous vertical magnetic field. Induction vectors are sensitive to lateral conductivity differences, however are comparatively insensitive to changes in resistivity with depth (Chave and Jones 2012).

Induction arrows are complex vectors which must have magnitude and direction as well as real and imaginary components. The orientation of induction vectors can be given in one of two conventions, Parkinson and Wiese conventions (Simpson and Bahr 2005). In this paper I have adopted the Parkinson convention in which induction arrows point towards more conductive regions.

In the Parkinson's convention there are two components to the induction vector (*M*), the real (*Re*) and the imaginary (*Im*) component of *T*. Each component has amplitude:

$$M_{Re}=\sqrt{Re(T_x)^2 + R(T_y)^2} \quad \text{and} \quad M_{Im} = \sqrt{Im(T_x)^2 + i(T_y)^2} \tag{4}$$

Directions of the real and imaginary arrows (positive clockwise from the geographic north) are given by:

$$\theta_{Re} = \arctan \frac{Re(T_y)}{Re(T_x)} \tag{5}$$

$$\theta_{Im} = \arctan \frac{Im(T_y)}{Im(T_x)}$$

R and *i* denote the real and imaginary parts of the transfer functions.

The trends of the induction vectors across different periods allow regional variations of conductivity to be detected. Real arrows (or vectors) will point directly towards regions of high conductivity.

OBSERVED DATA

Methods

Legacy GDS data have been compiled from various sources, including the Australia Wide Array of Geomagnetic Stations (AWAGS) survey, which comprised 58 GDS stations covering mainland Australia (Chamalaun and Barton 1990, Chamalaun and Barton 1993, Welsh et al. 1996). Of the 58 stations, 54 were portable three-component

magnetometers and four were permanent magnetic observations (Chamalaun and Walker, 1982). The geomagnetic field fluctuations were recorded at 1-minute intervals with 1 nT sensitivity combined with sensor temperature and time. Data recording commenced on the 18th of November 1989 and finished on the 17th of December 1990 (Welsh et al. 1996). Other GDS data has been sourced from studies conducted in Ballarat and Halls Creek (Milligan et al. 1993, Roberts et al. 2008). Details of the respective stations are given in Table 1.

Table 1 GDS sites including station number, code, latitude, longitude and elevation

Station	Station Code	Latitude	Longitude	Elevation (m)
Data: AWAGS (Welsh et al. 1993)				
47	ABY	-34.945	117.805	75
21	ALP	-23.655	146.587	420
18	ASP	-23.807	133.898	540
49	BAL	-34.624	143.573	64
26	BIR	-25.91	139.352	55
36	BUK	-30.052	145.952	117
45	CDN	-33.063	147.213	217
42	CED	-32.13	133.713	20
8	CKT	-15.477	145.187	6
54	CNB	-35.317	149.367	859
23	CNE	-25.803	122.945	452
7	CRO	-18.215	142.253	120
55	CTA	-20.083	146.25	370
33	CVN	-24.882	113.665	5
1	DAR	-12.403	130.859	31
9	DER	-17.37	123.663	5
5	DYW	-16.273	133.373	230
32	EMU	-28.63	132.198	300
48	ESP	-33.685	121.822	150
34	ETA	-28.718	138.633	300
41	EUC	-31.682	128.88	5
13	GER	-28.797	114.703	35
38	GFN	-29.767	153.02	27
24	GIL	-25.035	128.3	609
19	GLE	-2.883	138.817	158
57	GNA	-31.783	115.95	60
2	GOV	-12.377	136.74	50
15	GRN	-20.56	130.355	380
10	HAL	-18.233	127.667	440

14	HED	-20.377	118.63	4
12	ISA	-20.667	139.49	341
17	KIW	-22.867	127.55	450
30	LAV	-28.612	122.422	462
56	LRM	-22.217	114.1	4
58	MAC	-16.273	133.373	230
29	MEK	-26.61	118.545	518
44	MEN	-32.4	142.417	61
37	MOR	-29.498	149.847	230
25	MTD	-26.067	135.245	62
51	MYB	-25.523	152.728	10
46	NEW	-32.796	151.836	7
50	POL	-38.313	141.467	93
43	PTA	-32.483	137.75	5
27	QUI	-26.608	144.253	215
6	ROB	-16.717	136.95	80
28	ROM	-26.55	148.775	308
39	SOX	-31.239	119.355	345
11	TCK	-19.627	134.183	376
16	TEL	-21.705	122.228	293
35	TIB	-29.448	142.053	120
53	TOO	-37.533	145.467	457
52	TWO	-35.032	138.578	163
22	VER	-24.23	118.237	400
31	WAN	-28.51	129	310
1	WEI	-12.68	141.925	19
20	WTN	-22.367	143.082	215
4	WYN	-15.51	128.147	5
40	ZAN	-31.037	123.568	274
Data: Halls Creek (Roberts et al. 2008)				
31	EMG	-15.918	128.049	101
33	DUN	-16.013	128.429	78
39	ORD	-16.028	128.8	84
49	POP	-16.677	128.26	252
48	SPC	-16.719	128.92	175
34	NEG	-17.354	129	198
42	PUR	-17.411	128.202	301
54	PAN	-17.878	127.832	333
29	NIC	-18.033	128.993	386
22	FLO	-18.314	128.563	372
43	KOO	-18.455	127.581	467
47	LAM	-18.553	127.236	354
15	MAR	-18.635	126.968	320
16	RUB	-18.763	127.721	404
46	WOL	-19.088	127.672	363
Data: Ballarat (Milligan et al.1993)				
3	BAL	-37.583	143.743	455

11	BAL	-37.699	143.599	352
19	BAL	-37.725	143.736	459
99	BAL	-37.515	143.789	439
5	BAL	-37.597	143.580	388
14	BAL	-37.849	143.605	215
26	BAL	-37.726	143.911	389
37	BAL	-37.523	143.905	581
52	BAL	-37.011	143.015	218

The AWAGS, Ballarat and Halls Creek data were processed to industry standard Electrical Data Interchange (EDI) format using a robust bounded influence remote referencing method BIRRP; Bounded Influence, Remote Reference Processing (Chave and Thomson 2004). The EDI files were imported into WinGlink in order to create a map of regional GDS induction vectors across Australia at different periods.

Results

Using this method, induction vector maps were generated at four different periods; 1000 s, 3333 s, 5000 s and 10,000 s. Major differences were only apparent between periods of 1000 s and 10,000 s (Figure 1). These periods provide the opportunity to understand the regional scale conductivity contrasts throughout Australia. At 1000 s, the induction vectors along the coast of Western Australia are quite large, primarily due to the coast effect, in which conductive sea water causes vectors near the coast to point straight out to large bodies of seawater (Simpson and Bahr 2005, Nam et al. 2009, Yang et al. 2010). The induction vectors on the east coast of Australia also appear similar to the West Australian coastal vectors, both in magnitude and orientation. Throughout the centre of Australia and the major cratons, the induction vectors are smaller in magnitude and tend to point towards major sedimentary basins. This trend holds throughout the two different periods. The length of the induction vectors vary significantly over the

two periods, with obvious decrease in size around the Kimberly craton region at 10,000 s. There are no significant differences in the induction vectors surrounding the Australian coast between the two periods, however there is an extreme difference between the Charters Towers site over the two periods, highlighted in the red square in figure 1. The significantly large difference in the length of the induction vector is a unique case, and it may just be due to noise.

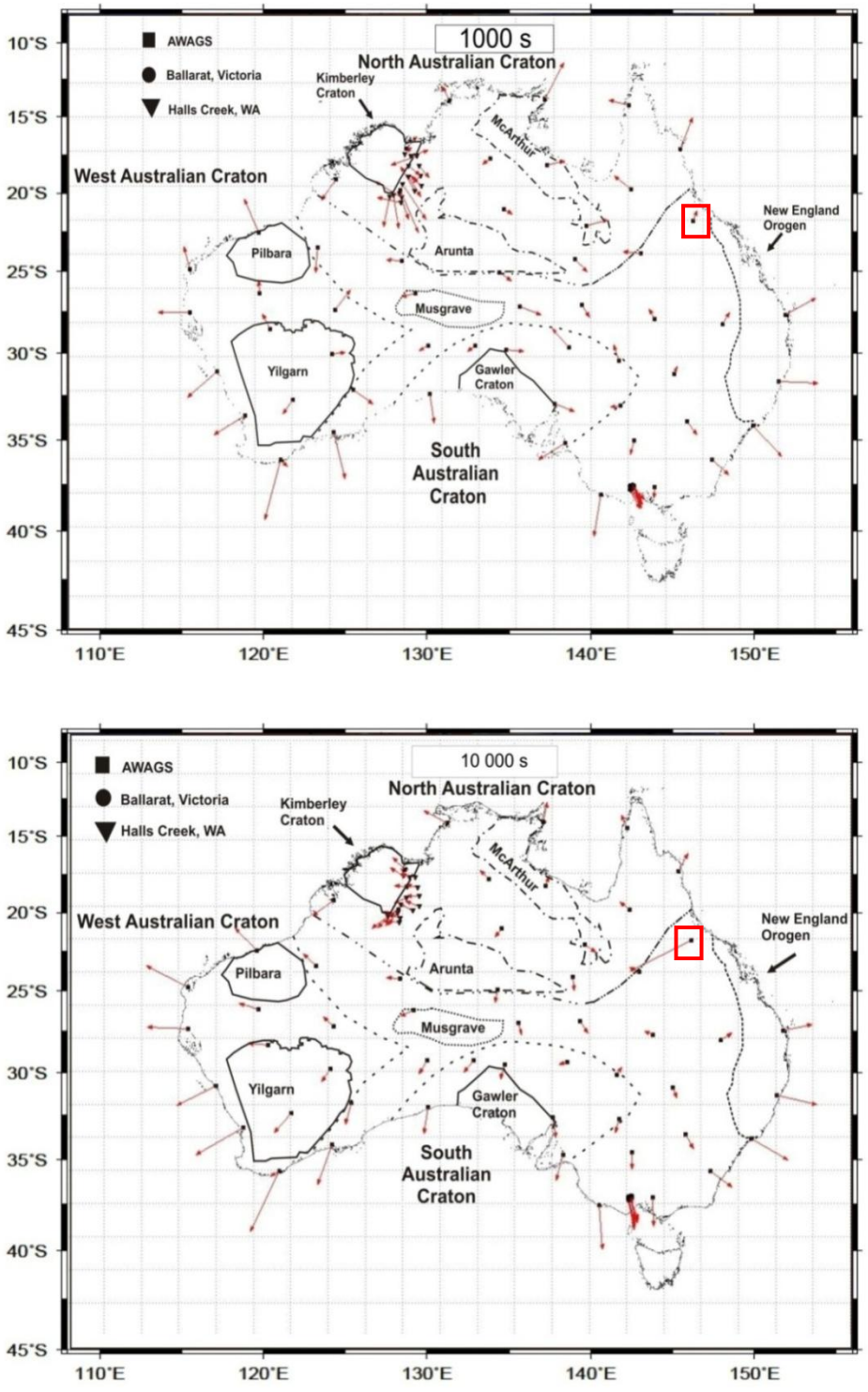

Figure 1 Real (or in-phase) induction vectors plotted on top of Australia's major cratons and basins using the Parkinson convention at periods of 1000 s and 10 000 s. The Charters Tower station, highlighted in the red square, is a region of notable change in the periods (adapted from Betts et al. 2002).

BUILDING AN AUSTRALIAN LITHOSPHERE RESISTIVITY MODEL

Surface Conductance: Methods

Conductance refers to the ability of a 3D medium to conduct electricity, calculated through the ratio of current which flows to the potential difference present (Simpson and Bahr 2005).

To produce a map of Australia's surface conductance, two constraints were used; SEEBASE, a present-day configuration of basement topography, which is consistent with the structural evolution of Phanerozoic basins, thus providing a quantitative, depth to basement model (FROGTECH 2012). The other constraint, ETOPO1, is a 1-arc-minute resolution global relief model of the Earth's surface, allowing the extraction of topographic and bathymetric data at given latitude and longitude (Pante and Simon-Bouhet 2013). The conductance was determined by using an approximate resistivity of 10 Ω.m for the sediments and $\frac{1}{3.2}$ Ω/m for seawater.

It is important to note that for periods greater than 100 s, the top 5 km of the Australian continent can be interpreted as an electrically-thin layer when compared to typical skin depths (e.g. for 100 Ω.m at 100 s, the skin-depth is 50 km). This allows us to incorporate all lateral changes into a map of electrical conductance due to the relatively thin nature of the crust.

The surface conductance (Figure 2) of the Australian continent combined with induction vectors allows us to compare observational and modelled data. Separating the surface conductance from the deeper crust helps to concentrate the deeper levels within the Australian mantle and to some extent determine the redox state.

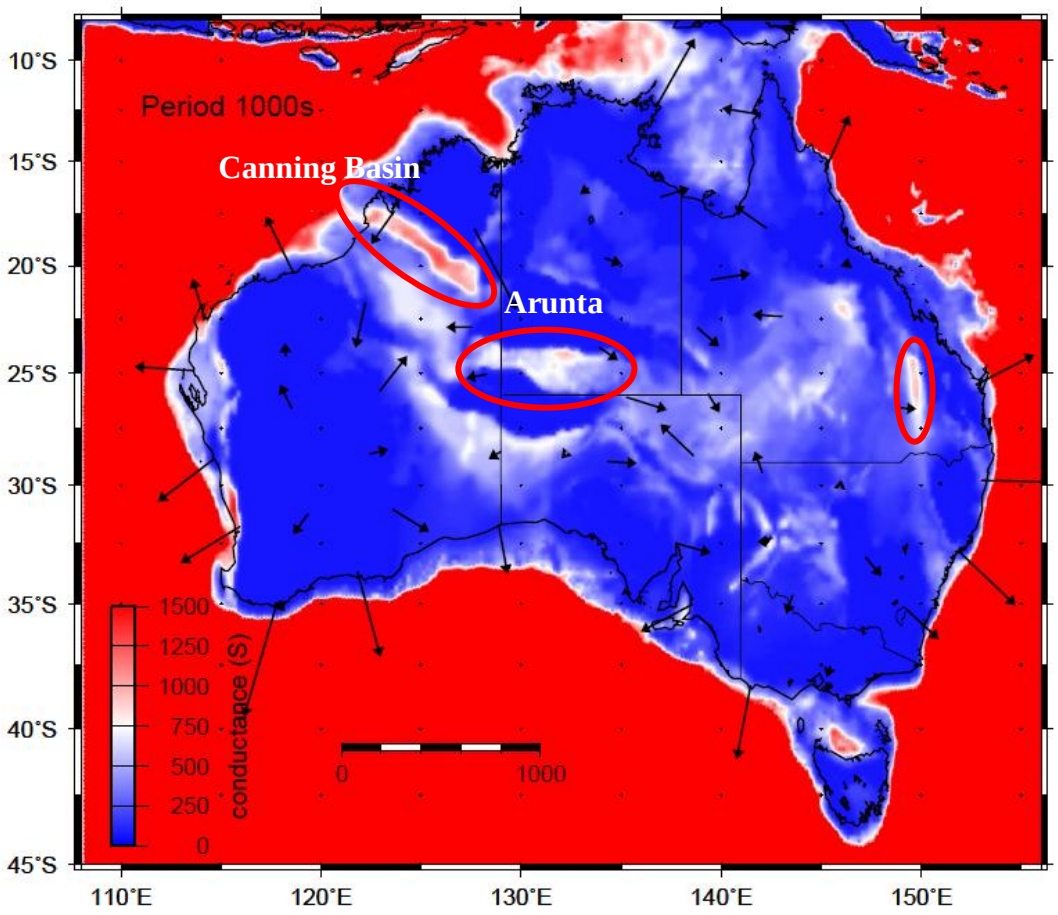

Figure 2 Surface conductance derived from depth to basement topography and water depth databases of the Australian continent with AWAGS induction vectors plotted at a period of 1000 s. Areas of notably high conductance have been highlighted with red circles, in particular the Canning Basin and the Arunta region.

Results

The induction vectors plotted on the surface conductance map image observational data, which is strongly correlated with the estimated surface conductance model. Regions of high conductance correlate strongly with known sedimentary basins, namely the Arunta and Musgrave region, as well as the Canning basin. Underneath Western Australia, the major cratons, Pilbara and Yilgarn cratons are highly resistive, similar to the Gawler Craton in South Australia (Maier et al. 2007, Thiel and Heinson 2013).

Mantle Lithosphere Resistivity: Methods

The Australian Seismological Reference Model (AuSREM) has been designed to capture a wide range of seismological information that has been generated over a number of decades (Kennett and Salmon 2012). The AuSREM model is based on a grid with 0.5º spacing in both latitude and longitude (approximately 50 km at the latitudes of Australia). For the upper mantle of Australia, the primary source of data is seismic surface wave tomography, combined with the analysis of body wave arrival times and regional tomography (Kennett et al. 2013). The model provides data in 25 km depth intervals from 75 to 300 km; the regional tomography allows accurate constraints to be put onto the relation between *P*- and *S*-wave speeds in the mantle lithosphere. The shallow structure of the Australian lithosphere in the AuSREM model has been developed using crustal data through the recent Moho study conducted by Kennett et al. (2011). The study used available sources of seismological information including sediment thickness, cross checks against recent reflection profiling, as well as providing *P* and *S* wavespeed distributions through the Australian crust. These were then taken to develop a comprehensive model of the Moho depth across Australia (Salmon et al. 2013).

Using AuSREM shear-wave velocity data (v_s), a linear relationship between the inverse logarithm of resistivity and v_s was empirically determined from Jones et al. (2013). The expression, developed from a robust linear regression of 1/logarithm (gridded resistivity) to v_s is applied to estimate the velocity at a given depth, expressed as follows:

$$v_s = 5.083 - 1.465/\log(\rho) \quad (6)$$

Values are taken from a cross plot of 1/logarithm of resistivity against v_s (Figure 3) from the SAMTEX experiment (Fullea et al. 2011).

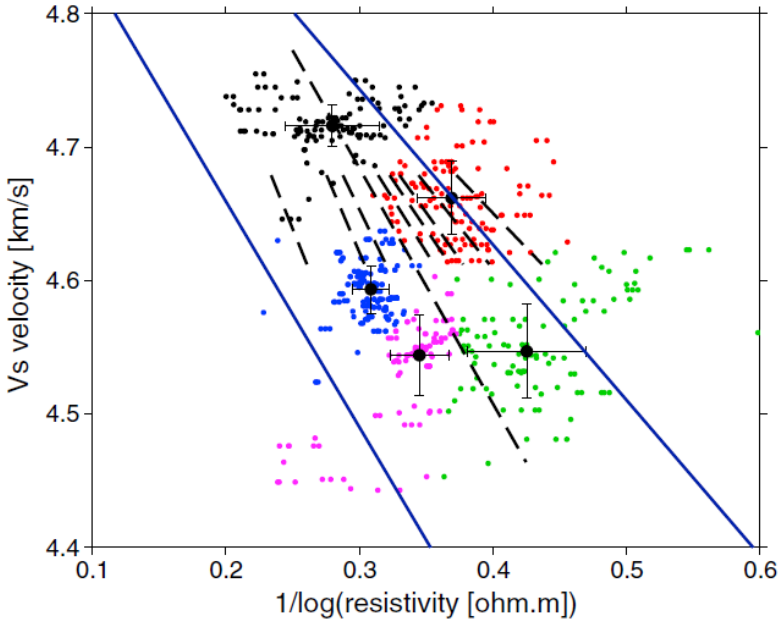

Figure 3 The fit to the cross plot of 1/log (resistivity) against shear wave velocity at five different cluster points represented by different colours. Each cluster point is fitted with a robust centroid represented by the black dots as well as error bars one standard deviation. Dashed black lines are inferences taken from a cross plot showing varying water content in major lithospheric minerals such as olivine. The blue lines represent expected extreme conditions such for water contents of 200, 300, and 0 in ppm for Opx, Cpx and Gt respectively. Adapted from Jones et al. (2013).

Rearranging equation 6:

$$\rho = 10 - \frac{1.465}{v_s - 5.083} \tag{7}$$

Applying equation 7 allows us to predict the relationship between v_s and electrical resistivity beneath Australia over a depth range of 50-150 km. Using v_s values from the AuSREM data set, the relationship was applied and resistivity was predicted at depths of 50 km and 100 km, shown in Figure 4.

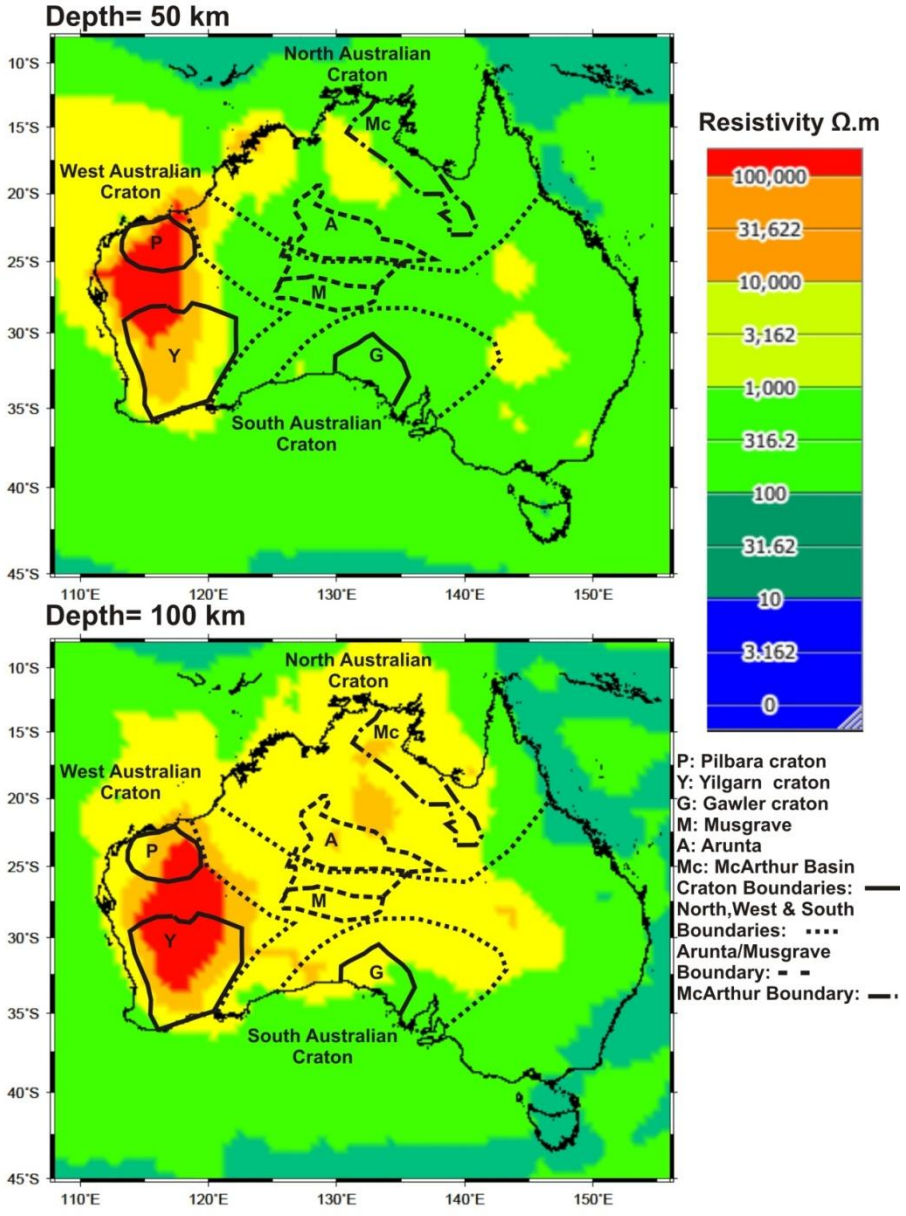

Figure 4 Map view of resistivities at depths of 50 km and 100 km with a spatial resolution of approximately 50 km, derived from the AuSREM shear-wave velocity and the empirical relationship equation from Jones et al. (2013). Location of cratons and basins are adapted from Betts et al. (2002)

Results

Regions of high resistivity show a strong relationship with known geological cratons and basins, most notably the Pilbara and Yilgarn cratons. With increasing depth from 50 to 100 km, the central Australia region becomes more resistive underneath the Arunta and Musgrave regions. Much of the east coast remains at a consistent range of 100 to 1000 Ω.m with increasing depth. It is apparent that the highly resistive West Australian regions correlate strongly with the observation data shown in Figure 1, in that induction vectors in Western Australia point towards the coast and away from the highly resistive bodies.

TESTING OBSERVATIONAL DATA

Thin Sheet Model: Methods

The thin sheet method was first developed by Price (1949) and involves to treating the electrically conductive surface of the Earth as thin, in order to solve 3D induction problems relating to the variations of conductance in a horizontal space, occurring in a thin sheet above a uniform half space (Heinson and Lilley 1993). Seawater is assumed to remain constant when compared with large geological variations in conductivity, allowing the conductance of the ocean to become a function of depth (Heinson and Lilley 1993). Having a sufficiently large skin depth allows a sheet of conductance to incorporate both basins and the ocean. The thin sheet is defined by thickness h, and local integrated conductance $\tau(x, y)$ at position (x, y). Beneath the thin sheet, the top layer is considered to have conductivity σ_1, thickness h_1 and EM skin depth δ at period T (Heinson and Lilley 1993).

Using the thin sheet method allows us to incorporate two pieces of data (where conductivity is best known); basins and oceans. Our thin layer (the top 5 km of Australia) contains complex variations in conductivity between 100 s and 10,000 s (Figure 5). This allowed us to determine the surface MT and GDS responses across Australia in a relatively high resolution thin-sheet (approximately 17 km by 17 km) ensuring that 250 nodes were covered between 108º to 156º degrees East and 8º to 47º degrees South.

Results

The outputs generated in the thin-sheet model shown in Figure 5 display maps of MT responses which are consistent with characteristics at 1000 s for MT rotated data. The apparent resistivity map in north-south orientation (x) and magnetic field orientated east-west (y) displays conductive bodies that are represented similarly in Figure 2. It is apparent from the thin-sheet modelling that MT responses across the country are varying, indicating that oceans and sedimentary basins have a major effect on MT responses. The thin-sheet model also shows that the induction vectors from the AWAGS experiment closely resemble the modelled responses.

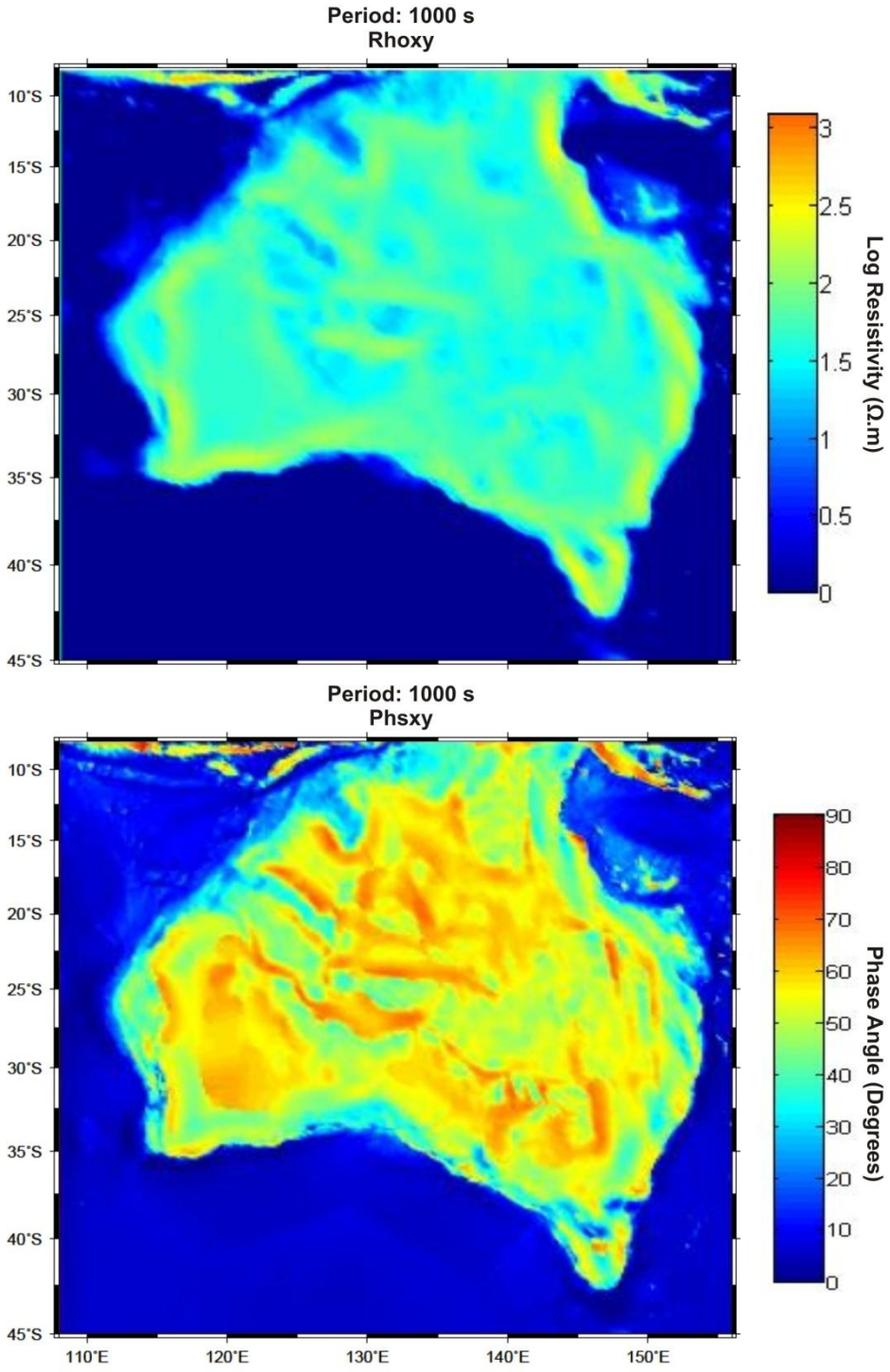

Figure 5 Apparent resistivity plotted at 1000 s with the electrical field in a north-south orientation (x) and the magnetic field in the east west orientation (y). Phase has been plotted in the same orientation for the Australian continent. Major sedimentary basins and the oceans surrounding Australia have a major effect on the MT responses, with known sedimentary basins clearly identifiable within the MT responses.

3D Forward Model: Methods

The 3D forward model of the Australian continent was produced using WinGlink, based on Mackie et al. (1993) algorithms. I used induction data from the nationwide survey conducted by AWAGS. The dimensions used in the 3D forward model were 108º E to 156º E and 8ºS to 47ºS, as well as using extra cells in order to smooth out the edges. Resistivity of seawater was set to 0.3 Ω.m. The horizontal layer in 5 to 10 km is defined by basic crystalline rock at 1000 Ω.m, followed by a layer from 10 to 37.5 km, defined as the lower crust and oceanic lithosphere, at 10,000 Ω.m. Between 37.5 to 62. 5 km resistivities have been derived from the AuSREM 50 km data set, continuing down to 150 km. Below this I have defined the asthenosphere as 100 Ω.m, the transition zone from 400-670 km as 10 Ω.m and the lower mantle as 1 Ω.m (Figure 6). The grid node spacing was 50 km on average.

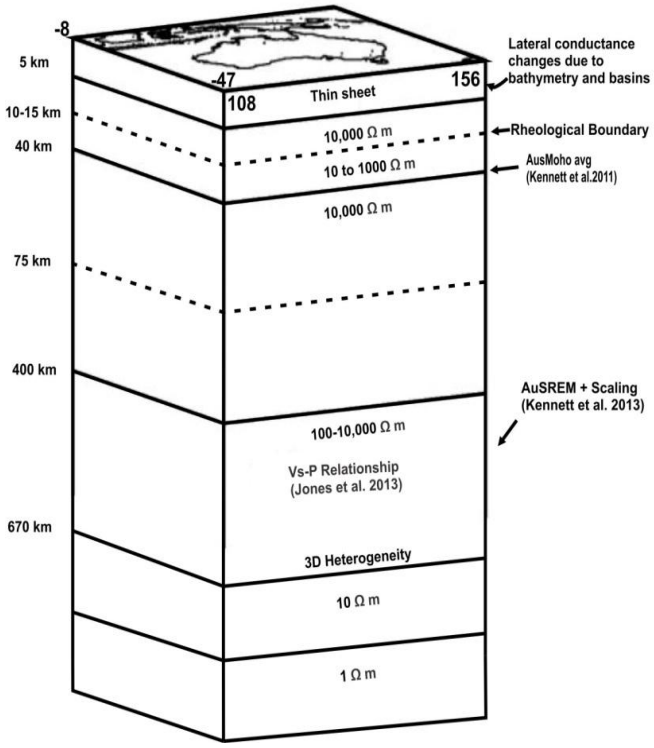

Figure 6 Parameters set for the 3D forward model and the raw data sets. Adapted from Wang and Lilley (1999).

Depth slices from the 3D forward model are shown in Figure 7, in comparison with induction vectors at a period of 1000 s.

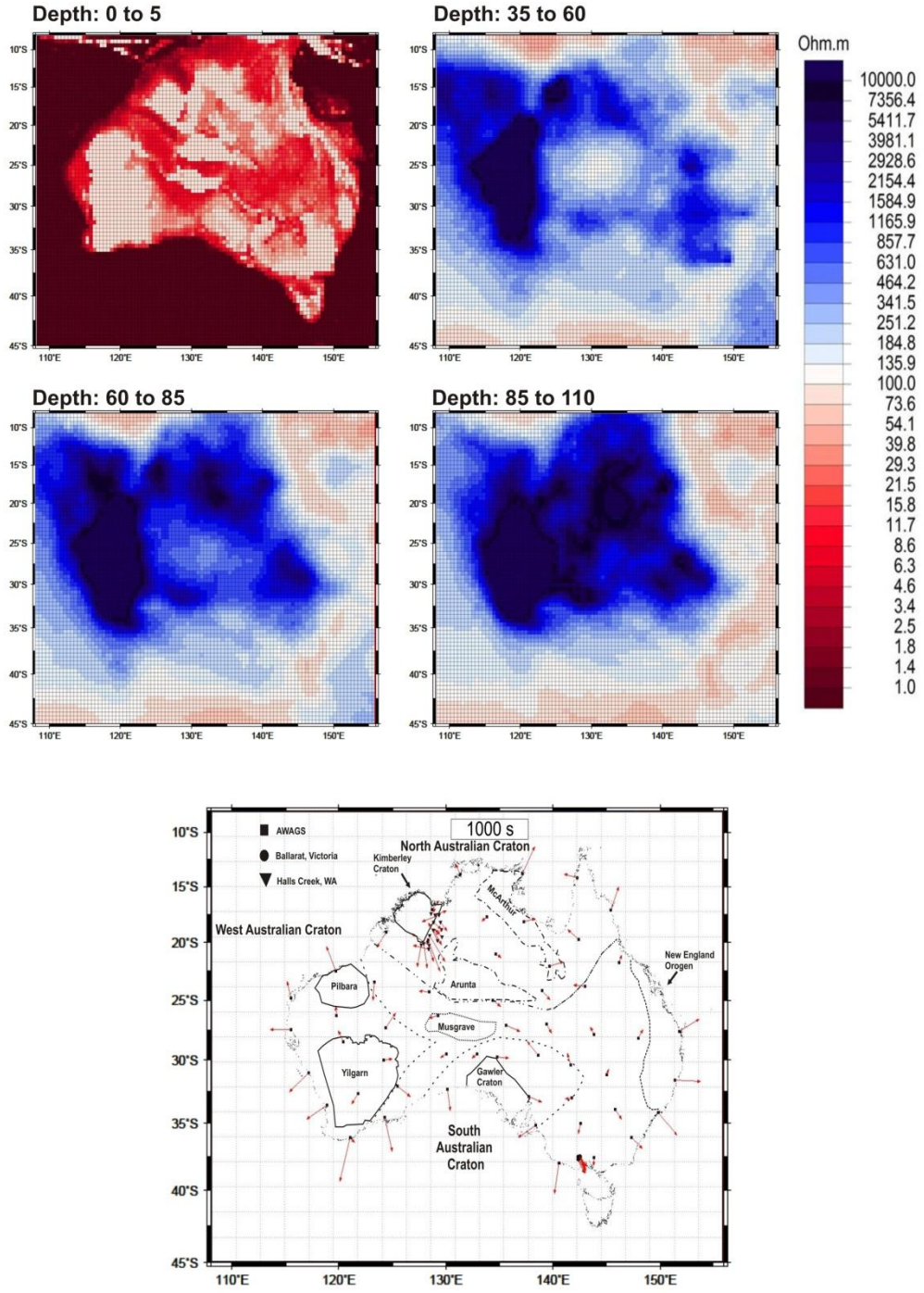

Figure 7 The 3D forward model of the Australian continent represented in map view from 0 to 5 km, 35 to 60 km, 60 to 85 km, and 85 to 110 km. Below is the observed induction vector data at a period of 1000 s for comparison.

Results

A large percentage of Western Australia consistently has a resistivity above 4000 Ω.m. With increasing depth, Central Australia, in particular the McArthur Basin becomes more resistive. The surface conductance model in Figure 2 shows a conductive region around the McArthur and Arunta regions. The forward model shows that beneath these regions, the lithosphere becomes increasingly resistive with depth. This conforms to the induction vectors plotted in Figure 1, with the increasing period induction vectors are pointing away from the Arunta and McArthur regions. Finally, in the 85 to 110 km depth slice, much of Australia appears to be highly resistive (1000 Ω.m or greater) throughout the whole lateral extent.

From the forward model I produced a map of modelled induction vectors at a period of 1000 s (Figure 8). The synthetic induction vector trend similarly to the AWAGS induction vectors, however there is an obvious decrease in vector size. The coastal vectors are both similar; predominantly along the west Australian coast as well as similar orientation, particularly throughout central Australia and inland from east Australian coast. Major differences are obvious between the two sets of data along the east coast of Australia, where the synthetic induction vectors are significantly smaller in size.

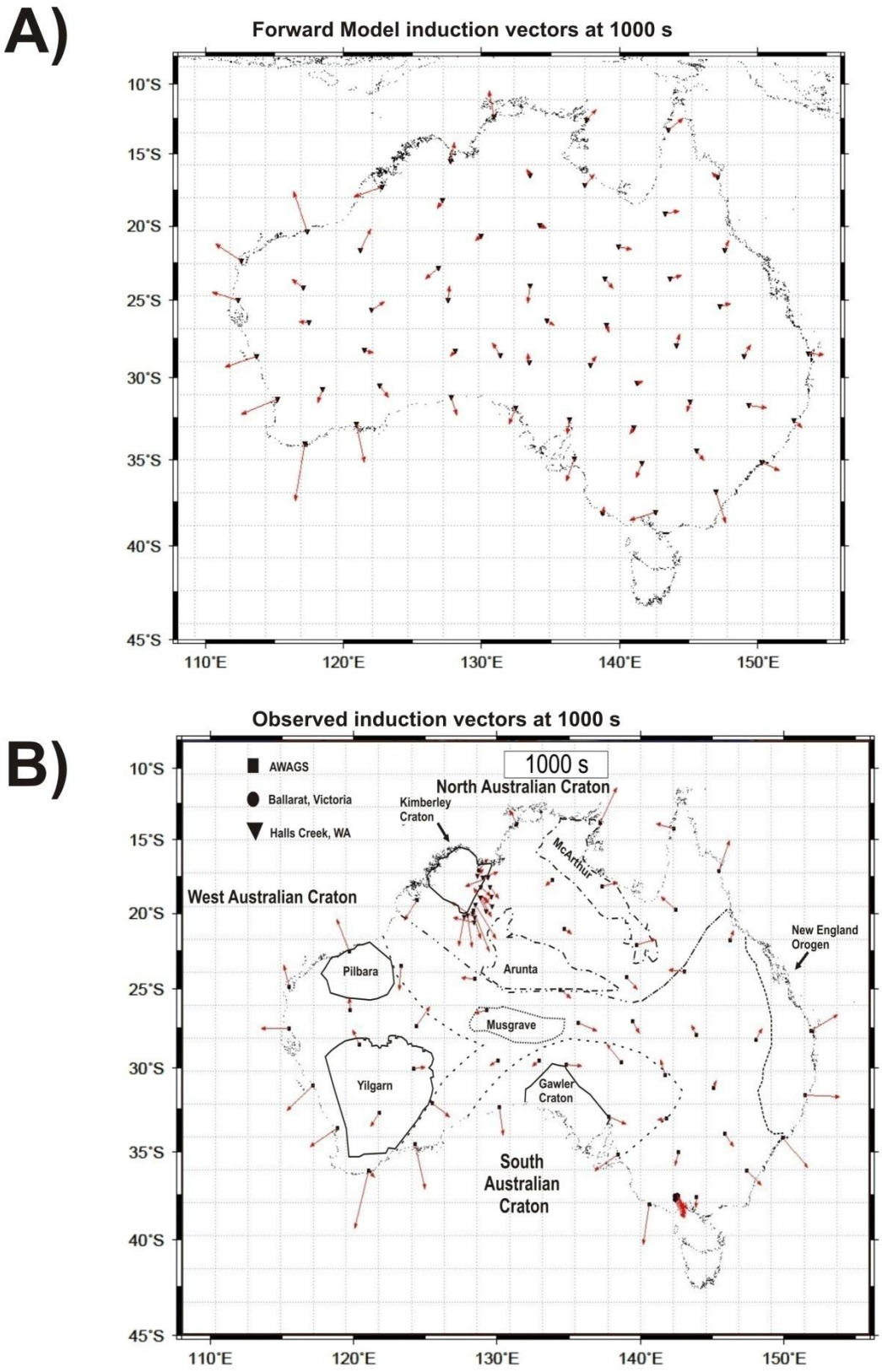

Figure 8 A) The forward model synthetic induction vectors plotted at 1000 s B) AWAGS induction vectors plotted at a period of 1000 s for comparison.

TESTING DATA

Thin-Sheet Inversion: Method

The thin-sheet inversion method has been adopted from Wang and Lilley (1999) using the conjugate gradient relaxation method, allowing us to optimize data misfit and model roughness. The main objective of using the thin-sheet inversion is to determine the distribution of electrical conductance within the thin sheet layer itself (Wang and Lilley 1999).

The thin-sheet inversion was produced from AWAGS data (Figure 8). The conductance values for the ocean surrounding Australia were kept fixed, primarily because conductance values are mainly influenced by sea water and the conductance values can be accurately calculated using depths from bathymetric charts. The surface grid for the model was set to 60 by 60 cells with each cell of side length 100 km (Wang and Lilley 1999). Of the 3600 cells within the grid, 137 cells hold observed data. The ocean conductance values were set, leaving 861 cells to be determined in the inversion process.

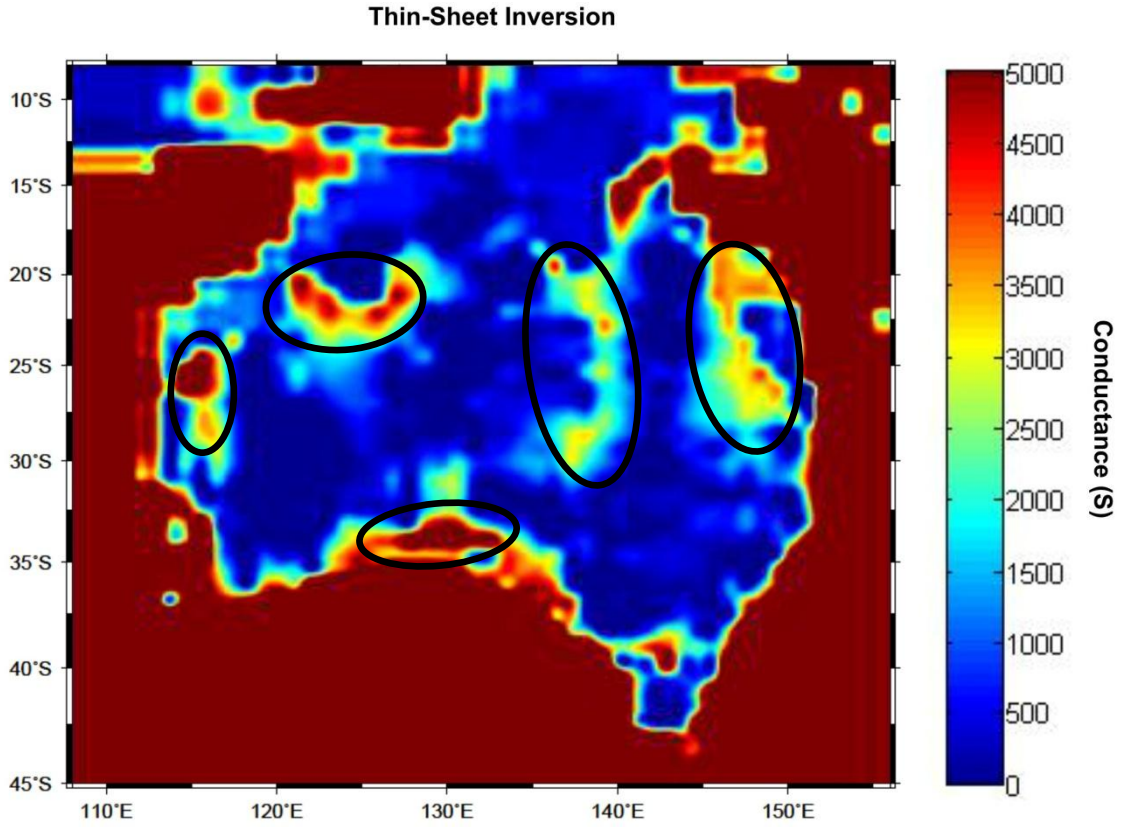

Figure 9 Thin-sheet Inversion of real or in-phase induction vectors at a period of 1000 s. The inversion reveals five regions of anomalous conductance structures which up to five times the conductance values as the continental background. These regions have been highlighted with black circles.

Results

The thin-sheet inversion reveals five anomalous conductive regions all over the Australian continent. Of particular interest is the conductive area along the west Australian coast, situated next to the resistive Pilbara craton and the conductive region along the South Australian coast within the Gawler craton. The three other major conductive regions are situated within known geological cratons and basins, including the Kimberley craton and the Arunta and Musgrave regions. These regions are strongly linked with the observational data shown in Figure 1.

DISCUSSION

Observational Data

Induction vectors are interpreted to be explained to the first order by the conduction in the oceans and major sedimentary basins. The contrasting differences between non sedimentary basins and the basins results in a decrease in the vector size when compared to the coastal vectors. Over the two periods the induction vectors hold similar trends, suggesting that with increasing period, or depth, the same deep resistivity structures are evident. The high conductivity of the ocean ensures that the coast effect influences the orientation and magnitude of the induction vectors along the Australian coastline (e.g. Nam et al. 2009). The coast effect refers to the sharp electrical contrast between the sea and the land, meaning the sea can have a substantial influence on the GDS responses, shown in Figure 1. The influence of the coast effect means that deeper structures within the crust and mantle may not have impacted the magnitude and orientation of the induction vectors. Similar results were produced in Chamalaun and Barton (1990) and Wang et al. (1997), whose induction vector plots displayed large induction vectors along the Australian coast, although at much lower periods than those produced in this paper.

Modelled Data

Both the surface conductance model and the thin-sheet inversion reveal similar conductive anomalies, most notably near the Kimberley craton and Charters Towers region. The inversion displayed conductive bodies similar to those seen in the surface conductance model as well revealing highly conductive structures along coastal areas which are often difficult to detect using induction vectors. Similar results can be found

in Wang et al. (1997) and Wang and Lilley (1999), whose models displayed the same conductive bodies, in particular along the Australian coast as well as the Canning Basin (Figure 2 and 9) . Thin-sheet modelling showed that the GDS responses across Australia are primarily affected by the surrounding oceans and major sedimentary basins. These results are comparable to Heinson and Lilley (1993) and Wang and Lilley (1999). The conductive anomalies seen in figures 2 and 9 could be the result of near-surface causes such as saline water or much deeper conduction mechanisms such as crustal mineralisation (e.g. graphite) or deeper molten material at mantle depths. The induction vectors in western Australia are consistent with the surface conductance model, which shows a highly resistive region stretching for most of the state with induction vectors influenced heavily by the highly conductive seawater, also known as the coast effect (Simpson and Bahr 2005).

The synthetic induction vectors seen in Figure 8 establish similar trends to the AWAGS induction vectors; however there is an obvious decrease in vector size. This suggests that conductivity trend in the synthetic data is much weaker than those seen in the AWAGS data. The weakening trend suggests that the forward model is missing deeper resistivity structures which are evident within the AWAGS data.

Comparison of Observational and Modelled Data

Observation and modelled data revealed that resistivity varies throughout Australia; regions of notably high resistivity are strongly correlated to the Western Australian Pilbara and Yilgarn cratons. The second order effects of resistivity variations in the deeper lithosphere are important, however the observed data become less sensitive to these with depth. It is also clear that MT (and GDS) responses are relatively sensitive to

structures which are less than one-skin depth thick. Conductive bodies located along the Australian coast, in particularly the west Australian coast, appear unrelated to any major sedimentary basins.

The 3D inversion shows that there are other additional crustal conductors which cannot be explained from sediment thickness alone and require additional conduction mechanisms in the crust over significant depths. The synthetic induction data from the forward model provides an ideal foundation to further develop an Australian lithosphere resistivity structure similar to those seen in Fullea et al. (2011) and Shen et al. (2013).

CONCLUSION

In this study I have developed models of electrical resistivity using various constraints and then tested these against known observations. It is clear that the surface conductance accounts for most of the long-period inductive responses seen across Australia. The second order effects of resistivity in the deeper crust are important however the sensitivity of induction vectors or observational data is less. It is also clear that additional crustal conductors cannot be explained from sediment thickness alone and must require another mechanism in the crust over significant depths. Further research could be centred on developing a continent wide magnetometer array, with a station spacing of 100 km or less. In areas where conductive anomalies are observed, decreasing station spacing will be required in order to produce more detailed electrical resistivity models of the Australian lithospheric structure.

ACKNOWLEDGMENTS

I acknowledge the help of Liejun Wang and his efforts with the thin-sheet inversion. I'd also like to thank Maptek and in particular Simon Ramsey for the imaging software and technical assistance with this software.

I would also like to thank my primary supervisor, Professor Graham Heinson, for his support, scientific input throughout the year and the opportunity to undertake Honours this year. Thank you also to Stephan Thiel, Lars Krieger and Kate Robertson for their efforts throughout the year.

REFERENCES

ARORA B. R.*, et al.* 1999 Overview of Geomagnetic Deep Soundings (GDS) as applied in the parnaíba Basin, North-Northeast Brazil, *Revista Brasileira de Geofisica,* vol. 17, no. 1, pp. 41-65.

BEDROSIAN P. A. & FEUCHT D. W. 2013 Structure and tectonics of the northwestern United States from EarthScope USArray magnetotelluric data, *Earth and Planetary Science Letters*.

BETTS P. G.*, et al.* 2002 Evolution of the Australian lithosphere, *Australian Journal of Earth Sciences,* vol. 49, no. 4, pp. 661-695.

CHAMALAUN F. & BARTON C. 1990 Comprehensive Mapping of Australia's Geomagnetic Variations, *Eos, Transactions American Geophysical Union,* vol. 71, no. 51, pp. 1867-1873.

CHAMALAUN F. H. & BARTON C. E. 1993 Electromagnetic induction in the Australian crust: results from the Australia-wide array of geomagnetic stations, *Exploration Geophysics,* vol. 24, no. 2, pp. 179-186.

CHAVE A. D. & JONES A. G. 2012 The Magnetotelluric Method: Theory and Practice. Cambridge University Press.

CHAVE A. D. & THOMSON D. J. 2004 Bounded influence magnetotelluric response function estimation, *Geophysical Journal International,* vol. 157, no. 3, pp. 988-1006.

EATON D. W.*, et al.* 2009 The elusive lithosphere–asthenosphere boundary (LAB) beneath cratons, *Lithos,* vol. 109, no. 1, pp. 1-22.

EVANS R. L.*, et al.* 2011 Electrical lithosphere beneath the Kaapvaal craton, southern Africa, *Journal of Geophysical Research B: Solid Earth,* vol. 116, no. 4.

FISHWICK S. & RAWLINSON N. 2012 3-D structure of the Australian lithosphere from evolving seismic datasets, *Australian Journal of Earth Sciences,* vol. 59, no. 6, pp. 809-826.

FROGTECH 2012 OZ SEEBASE

FULLEA J., MULLER M. & JONES A. 2011 Electrical conductivity of continental lithospheric mantle from integrated geophysical and petrological modeling: Application to the Kaapvaal Craton and Rehoboth Terrane, southern Africa, *Journal of Geophysical Research: Solid Earth (1978–2012),* vol. 116, no. B10.

HEINSON G. S., DIREEN N. G. & GILL R. M. 2006 Magnetotelluric evidence for a deep-crustal mineralizing system beneath the Olympic Dam iron oxide copper-gold deposit, southern Australia, *Geology,* vol. 34, no. 7, pp. 573-576.

HEINSON G. S. & LILLEY F. E. M. 1993 An application of thin-sheet electromagnetic modelling to the Tasman Sea, *Physics of the Earth and Planetary Interiors,* vol. 81, no. 1-4, pp. 231-251.

JONES A. G. 1999 Imaging the continental upper mantle using electromagnetic methods. pp. 57-80.

JONES A. G., EVANS R. L. & EATON D. W. 2009 Velocity–conductivity relationships for mantle mineral assemblages in Archean cratonic lithosphere based on a review of laboratory data and Hashin–Shtrikman extremal bounds, *Lithos,* vol. 109, no. 1, pp. 131-143.

JONES A. G., *et al.* 2013 Velocity-conductivity relations for cratonic lithosphere and their application: Example of Southern Africa, *Geochemistry, Geophysics, Geosystems,* vol. 14, no. 4, pp. 806-827.

JONES A. G., *et al.* 2012 Water in cratonic lithosphere: Calibrating laboratory-determined models of electrical conductivity of mantle minerals using geophysical and petrological observations, *Geochemistry, Geophysics, Geosystems,* vol. 13, no. 6, p. Q06010.

JONES A. G., *et al.* 2005 The electrical resistivity structure of Archean to Tertiary lithosphere along 3200 km of SNORCLE profiles, northwestern Canada, *Canadian Journal of Earth Sciences,* vol. 42, no. 6, pp. 1257-1275.

KARATO S.-I. 2010 Rheology of the Earth's mantle: A historical review, *Gondwana Research,* vol. 18, no. 1, pp. 17-45.

KARATO S.-I. & WU P. 1993 Rheology of the upper mantle: A synthesis, *Science,* vol. 260, no. 5109, pp. 771-778.

KELBERT A., EGBERT G. D. & DEGROOT-HEDLIN C. 2012 Crust and upper mantle electrical conductivity beneath the Yellowstone Hotspot Track, *Geology,* vol. 40, no. 5, pp. 447-450.

KENNETT B. L. N., *et al.* 2013 Australian seismological referencemodel (AuSREM): Mantle component, *Geophysical Journal International,* vol. 192, no. 2, pp. 871-887.

KENNETT B. L. N. & SALMON M. 2012 AuSREM: Australian Seismological Reference Model, *Australian Journal of Earth Sciences,* vol. 59, no. 8, pp. 1091-1103.

KENNETT B. L. N., *et al.* 2011 AusMoho: The variation of Moho depth in Australia, *Geophysical Journal International,* vol. 187, no. 2, pp. 946-958.

MACKIE R. L., MADDEN T. R. & WANNAMAKER P. E. 1993 Three-dimensional magnetotelluric modeling using difference equations - theory and comparisons to integral equation solutions, *Geophysics,* vol. 58, no. 2, pp. 215-226.

MAIER R., *et al.* 2007 A 3D lithospheric electrical resistivity model of the Gawler Craton, Southern Australia, *Transactions of the Institutions of Mining and Metallurgy, Section B: Applied Earth Science,* vol. 116, no. 1, pp. 13-21.

MILLIGAN P. R.*, et al.* 1993 Micropulsation and induction array study near Ballarat, Victoria, *Exploration Geophysics,* vol. 24, no. 2, pp. 117-122.

NAM M. J.*, et al.* 2009 Three-dimensional topographic and bathymetric effects on magnetotelluric responses in Jeju Island, Korea, *Geophysical Journal International,* vol. 176, no. 2, pp. 457-466.

O'REILLY S. Y. & GRIFFIN W. 2010 The continental lithosphere–asthenosphere boundary: Can we sample it?, *Lithos,* vol. 120, no. 1, pp. 1-13.

PANTE E. & SIMON-BOUHET B. 2013 marmap: A Package for Importing, Plotting and Analyzing Bathymetric and Topographic Data in R, *PLoS ONE,* vol. 8, no. 9.

PESLIER A. H.*, et al.* 2010 Olivine water contents in the continental lithosphere and the longevity of cratons, *Nature,* vol. 467, no. 7311, pp. 78-81.

POMMIER A. 2013 Interpretation of Magnetotelluric Results Using Laboratory Measurements, *Surveys in Geophysics*, pp. 1-44.

POUDJOM DJOMANI Y. H.*, et al.* 2001 The density structure of subcontinental lithosphere through time, *Earth and Planetary Science Letters,* vol. 184, no. 3-4, pp. 605-621.

PRICE A. T. 1949 The induction of electric currents in non-uniform thin sheets and shells, *Quarterly Journal of Mechanics and Applied Mathematics,* vol. 2, no. 3, pp. 283-310.

ROBERTS A.*, et al.* 2008

An electromagnetic investigation of the Halls Creek Orogen. Earth and Environmental Sciences*.* pp. 1-31. Adelaide University

SALMON M., KENNETT B. L. N. & SAYGIN E. 2013 Australian seismological referencemodel (AuSREM): Crustal component, *Geophysical Journal International,* vol. 192, no. 1, pp. 190-206.

SELWAY K. 2013 On the Causes of Electrical Conductivity Anomalies in Tectonically Stable Lithosphere, *Surveys in Geophysics*, pp. 1-39.

SHEN W., RITZWOLLER M. H. & SCHULTE-PELKUM V. 2013 A 3-D model of the crust and uppermost mantle beneath the Central and Western US by joint inversion of receiver functions and surface wave dispersion, *Journal of Geophysical Research B: Solid Earth,* vol. 118, no. 1, pp. 262-276.

SIMPSON F. & BAHR K. 2005 Practical Magnetotellurics*.* Cambridge University Press.

THIEL S. & HEINSON G. 2013 Electrical conductors in Archean mantle-Result of plume interaction?, *Geophysical Research Letters,* vol. 40, no. 12, pp. 2947-2952.

VOZOFF K. 1990 Magnetotellurics: Principles and practice, *Proceedings of the Indian Academy of Sciences - Earth and Planetary Sciences,* vol. 99, no. 4, pp. 441-471.

WANG D.*, et al.* 2006 The effect of water on the electrical conductivity of olivine, *Nature,* vol. 443, no. 7114, pp. 977-980.

WANG L. J. & LILLEY F. E. M. 1999 Inversion of magnetometer array data by thin-sheet modelling, *Geophysical Journal International,* vol. 137, no. 1, pp. 128-138.

WANG L. J., LILLEY F. E. M. & CHAMALAUN F. H. 1997 Large-scale electrical conductivity structure of Australia from magnetometer arrays, *Exploration Geophysics,* vol. 28, no. 2, pp. 150-155.

WELSH W., BARTON C. E. & ORGANISATION A. G. S. 1996 The Australia-Wide Array of Geomagnetic Stations (AWAGS): Data Corrections. Australian Geological Survey Organisation.

Y. O'RELLY S. & GRIFFIN W. L. 1985 A xenolith-derived geotherm for southeastern australia and its geophysical implications, *Tectonophysics,* vol. 111, no. 1-2, pp. 41-63.

YANG J., MIN D. J. & YOO H. S. 2010 Sea effect correction in magnetotelluric (MT) data and its application to MT soundings carried out in Jeju Island, Korea, *Geophysical Journal International,* vol. 182, no. 2, pp. 727-740.

YOSHINO T.*, et al.* 2009 The effect of water on the electrical conductivity of olivine aggregates and its implications for the electrical structure of the upper mantle, *Earth and Planetary Science Letters,* vol. 288, no. 1, pp. 291-300.

YOSHINO T.*, et al.* 2006 Hydrous olivine unable to account for conductivity anomaly at the top of the asthenosphere, *Nature,* vol. 443, no. 7114, pp. 973-976.

ZHDANOV M. S.*, et al.* 2011 Three-dimensional inversion of large-scale EarthScope magnetotelluric data based on the integral equation method: Geoelectrical imaging of the Yellowstone conductive mantle plume, *Geophysical Research Letters,* vol. 38, no. 8.